Supplementary Information

Assembling ultrathin $Ni(OH)_2$ nanosheets on poly(triazine imide) crystal hollow tubes for efficient CO_2 photoreduction

Keshan Tang[a], Fujia Zhang[b], Lei Zeng[a], Jingfang Zhang[a], Yang Xia[a,*], Xianglin Xiang[b*], Ruchun Li[c,*]

[a] State Key Laboratory of Green and Efficient Development of Phosphorus Resources, Key Laboratory of Green Chemical Engineering Process of Ministry of Education, Hubei Key Lab of Novel Reactor and Green Chemical Technology, School of Chemical Engineering and Pharmacy, Wuhan Institute of Technology, Wuhan, 430072, China.

[b] Faculty of Materials Science and Engineering, Kunming University of Science and Technology, Kunming, 650093, China

[c.] Yunnan Key Laboratory of Modern Separation Analysis and Substance Transformation, College of Chemistry and Chemical Engineering, Yunnan Normal University, Kunming, 650500, China.

S1. Experimental section

1.1 Characterization:

The morphology of the samples was characterized by scanning electron microscopy (SEM) on JSM-7500F electron microscope (JEOL, Japan). Morphological observation was further visualized by the transmission electron microscopy (TEM, JEOL JEM-200. The powder X-ray diffraction (XRD) pattern was recorded using a Malvern Panalytical Empyrean diffractometer with Cu Kα radiation operated at 40 kV and 40 mA. X-ray photoelectron spectroscopy (XPS) measurements were performed using an ultrahigh vacuum VG EXCALAB 210 electron spectrometer with the excitation source of monochromatized Al Kα. The Fourier transform infrared (FT-IR) spectra of the samples were recorded using a NICOLET iS50 spectrometer. To measure the IR spectra, the samples were mixed with KBr and pressed into tablets for analysis (sample : KBr = 1: 100). Photoelectrochemical measurements were performed on a Shanghai Chenhua electrochemical workstation using a standard three-electrode cell with a working electrode (ITO glass), a platinum wire counter electrode and an Ag/AgCl reference electrode. The visible light source was obtained by using a 300 W Xenon lamp source (Microsolar 300) The sample powder (3 mg) was dispersed in 2 mL aqueous solution with H_2O: Ethanol: ACN= 42: 33 :1 (v/v/v) and the resulting suspension was evenly coated on a 0.8×0.8 cm^2 ITO glass, then dried at Ambient Air Drying before being used as a working electrode. The electrolyte solution is 0.5 M Na_2SO_4. UV-vis diffuse reflectance spectra (DRS) were investigated by a UV-vis spectrophotometer (UV-2600, Shimadzu, Japan) using $BaSO_4$ powder as a reference standard. The Brunauer-Emmett-Teller (BET) surface area was carried by BSD-660MG A6S|B3MG nitrogen adsorption apparatus. All the samples were

degassed at 100 ℃ before nitrogen adsorption measurements. Photoluminescence (PL) spectra were employed on HITACHI F-7000 FL Spectrophotometer. Time-resolved fluorescence emission spectra (TRPL) were surveyed by a FLS 1000 fluorescence lifetime spectrophotometer (Edinburgh Instruments, UK). Electron paramagnetic resonance (EPR) was measured using a Bruker E500 electron paramagnetic resonance spectrometer.

1.2 Theoretical simulation

Computational details: All the calculations were executed within the framework of density functional theory (DFT) method implemented in the Cambridge Serial Total Energy Package (CASTEP) codes. The exchange-correlation potential was described by the Generalized Gradient Approximation (GGA) with Perdewe-Burkee-Ernzerhof functional (PBE). The plane wave and ultrasoft pseudopotential method was used to account for core-valence interactions. The Kohn−Sham wave functions were expanded with an energy cutoff of 340 eV, and Gamma-centered scheme was employed with a K-point grid sample separation of 0.07 $Å^{-1}$ for the irreducible Brillouin zone. A vacuum of approximately 20 Å was placed above the slabs to separate the interaction between periodic images. The self-consistent field tolerance was set as 1×10^{-6} eV for solving the electronic wave function. The Broyden-Fletcher-Goldfarb-Shanno (BFGS) scheme Dwas chosen as the minimization algorithm. Convergence criteria for geometry optimization were set as follows: atomic forces were kept below 0.01 eV/Å, atomic stress was limited to 0.02 GPa, atomic displacement was restricted to less than 1×10^{-3} Å, and the energy change per atom was kept below 1×10^{-5} eV[1]. A Van der Waals DFT-D3 method was applied to accurately describe Van der Waals forces between layers. The DFT+U method was used to treat the on-site Coulomb correlation of Ni *3d* electrons, and the Hubbard parameter U is set to 2.5 eV. Spin-polarized calculations were applied in all the cases.

1.3 Average decay time (τ_{ave}):

The TRPL decay curves were fitted by the following triple-exponential equation[2]

$$I(t) = I_0 + B_1\exp\left(-\frac{t}{\tau_1}\right) + B_2\exp\left(-\frac{t}{\tau_2}\right) + B_3\exp\left(-\frac{t}{\tau_3}\right)$$

Respectively, The τ_{ave} of the photogenerated carriers was calculated by the following formula[3]:

$$\tau_{ave} = \frac{B_1\% \times \tau_1^2 + B_2\% \times \tau_2^2 + B_3\% \times \tau_3^2}{B_1\% \times \tau_1 + B_2\% \times \tau_2 + B_3\% \times \tau_3}$$

Where B_1, B_2 and B_3 represent the amplitudes of the fast, medium and slow components, τ_1, τ_2 and τ_3 represent the time constants.

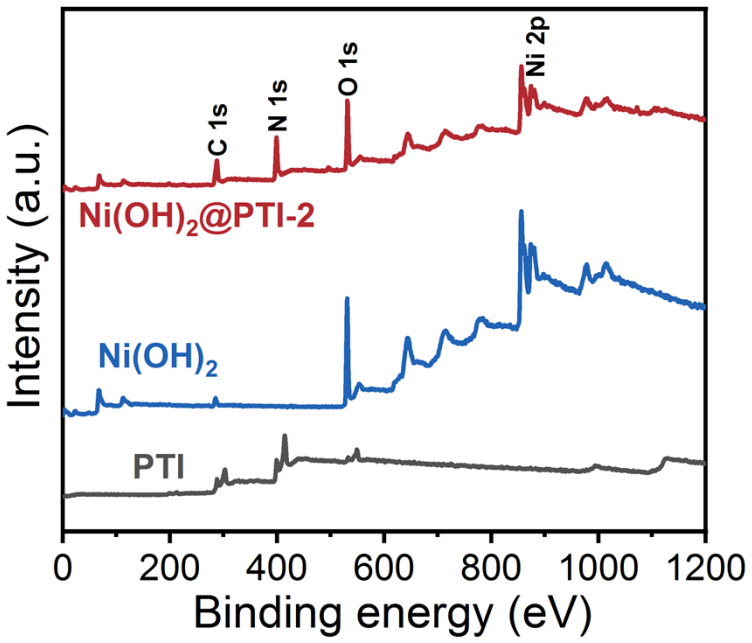

Fig. S1. XPS survey spectra of PTI, $Ni(OH)_2$ and $Ni(OH)_2$@PTI composite.

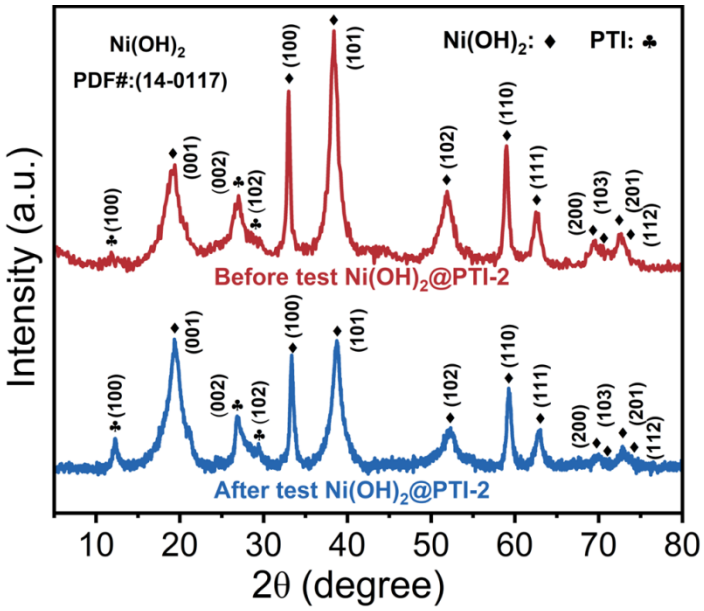

Fig. S2. X-ray diffraction (XRD) patterns of $Ni(OH)_2$@PTI-2 before and after photocatalytic cyclic experiment.

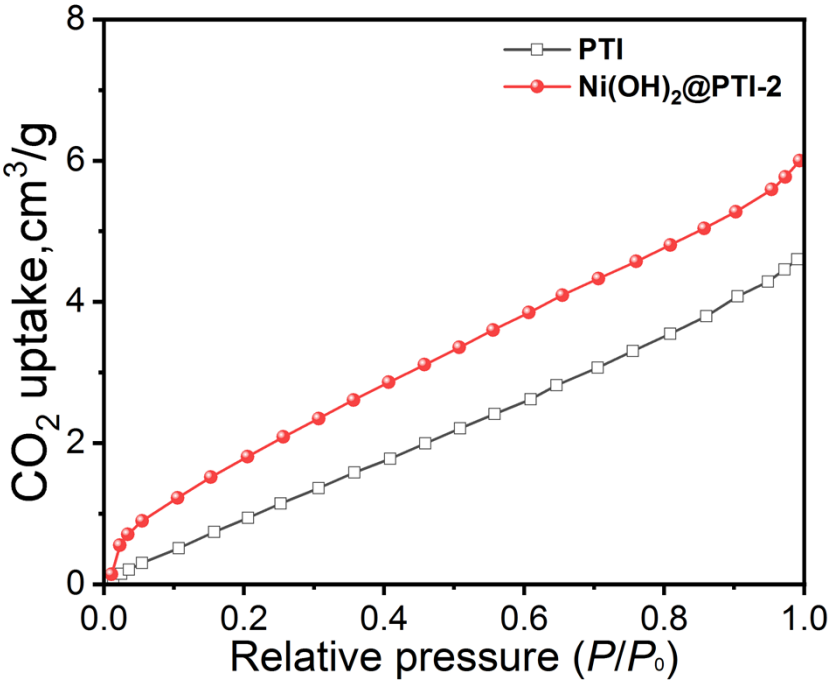

Fig. S3 CO_2 adsorption isotherms of PTI and $Ni(OH)_2$@PTI-2 composite at 273 K.

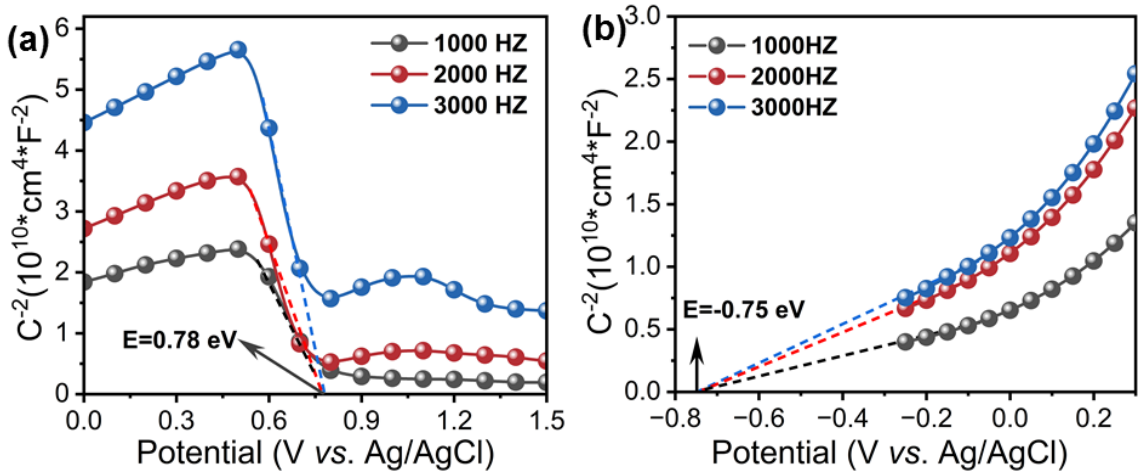

Fig. S4. Mott-Schottky curves of (a) PTI and (b) $Ni(OH)_2$ at different frequency in 0.5 M Na_2SO_4 solution.

Table S1. Specific surface areas pore volume and average pore size of MS, $Ni(OH)_2$ and $Ni(OH)_2$@MS composite.

Samples	**S_{BET} ($m^2 \cdot g^{-1}$)**	**Pore volume ($cm^3 \cdot g^{-1}$)**	**Average pore size (nm)**
MS	68.7	0.268	14.5
$Ni(OH)_2$	177.7	0.325	22.3
$Ni(OH)_2$@MS-0.5	76.3	0.271	10.4
$Ni(OH)_2$@MS-1	115.0	0.352	9.5
$Ni(OH)_2$@MS-2	140.4	0.426	9.6
$Ni(OH)_2$@MS-3	137.4	0.399	9.0

Table S2 Comparison of photocatalytic CO_2 reduction performance with others g-C_3N_4-based composite photocatalysts.

Photocatalysts	Reaction Solution	Light Source	CO ($\mu M\ g^{-1}\ h^{-1}$)	Reference
g-C_3N_4/rGO/NiAl-LDHs	H_2O: CH_3CN: TEOA: =1: 3: 3 (v/v)	300 W Xe lamp (780nm ≥ λ ≥ 320nm)	2.6	4
CN/LRSTO-30wt%	pure water	300 W Xe lamp (780nm ≥ λ ≥ 320nm)	4.1	5
WOx/Pt-g-C_3N_4	pure water	300 W Xe lamp (λ ≥ 420nm)	5.9	6
BiOBr/TCN	pure water	300 W Xe lamp (λ ≥ 400 nm)	10.9	7
$Bi_{19}S_{27}Br_3$/g-C_3N_4	pure water	300 W Xe lamp (780nm ≥ λ ≥ 320nm)	12.9	8
Cu-CuO_x /g-C_3N_4	H_2O: EtOH=10:1 (v/v)	300 W Xe lamp (780nm ≥ λ ≥ 320nm)	14.5	9
Cu-CNNTs	pure water	300 W Xe lamp (780nm ≥ λ ≥ 320nm)	16.1	10
g-C_3N_4/Cu_2SnS_3	pure water	300 W Xe lamp (780nm ≥ λ ≥ 320nm	18.2	11
Co/7-CN	pure water	300 W Xe lamp (λ ≥ 420nm)	19.1	12
PBUH/CN	pure water	300 W Xe lamp (780nm ≥ λ ≥ 320nm)	22.5	13
$Ni(OH)_2$@PTI-2	H_2O: ACN= 9: 1 (v/v)	300 W Xe lamp (780nm ≥ λ ≥ 320nm)	20.8	this work

Table S3 The fitted parameters obtained from decay curves of PTI and $Ni(OH)_2$@PTI-2 composite.

Sample	τ_1(ns) (Rel. %)	τ_2(ns) (Rel. %)	τ_3(ns) (Rel. %)	τ_A/ns
PTI	0.5 (61.9%)	3.3 (18.1%)	16.4 (20.0%)	13.98
$Ni(OH)_2$@PTI-2	0.3 (56.7%)	3.5 (27.1%)	26.1 (16.2%)	7.01

References

[1] Y. T. Que, R. M. Zhu, Y. Liu, Y. O. He, W. K. Han, H. Pang, J. Zhang, Z. G. Gu, *Angew Chem Int Ed Engl* **2025**, e15511.

[2] Y. Xia, H. Yang, W. Ho, B. Zhu, J. Yu, *Applied Catalysis B: Environment and Energy* **2024**, *344*.

[3] F. Wang, J. Xu, Z. Wang, Y. Lou, C. Pan, Y. Zhu, *Applied Catalysis B: Environmental* **2022**, *312*.

[4] D. Zhou, J. Zhang, Z. Jin, T. Di and T. Wang, *Chemical Engineering Journal*, 2022, **450**, 138108

[5] S. Wan, Y. Hou, W. Wang, G. Q. Luo, C. Wang, R. Tu and S. Cao, *Rare Metals*, 2024, **43**, 5880-5890.

[6] X. Zhang, K. Matras-Postolek, P. Yang and S. Jiang, *Carbon*, 2023, **214**, 118337.

[7] W. Tao, Q. Tang, J. Hu, Z. Wang, B. Jiang, Y. Xiao, R. Song and S. Guo, *Journal of Materials Chemistry A*, 2023, **11**, 24999-25007.

[8] J. Zhao, M. Ji, H. Chen, Y. Weng, J. Zhong, Y. Li, S. Wang, Z. Chen, J. Xia and H. Li, *Applied Catalysis B: Environment and Energy*, 2022, **307**, 121162.

[9] D. Wen, N. Wang, J. Peng, T. Majima and J. Jiang, *Journal of Materials Science & Technology*, 2025, **226**, 93-108.

[10] M. Chen, H. Li, Z. Shen, Q. Qu, W. Yang and J. Sun, *Chemical Engineering Journal*, 2023, **476**, 146836.

[11] H. Omr, R. Putikam, S. Feng, M. Lin and H. Lee, *Applied Catalysis B: Environmental*, 2023, **339**, 123103.

[12] H. Lin, J. Sun, M. He and G. Wang, *Journal of Materials Chemistry A*, 2025, **13**, 10855-10862.

[13] M. Hussien, A. Sabbah, M. Qorbani, R. Putikam, S. Kholimatussadiah, D. Tzou, M. Elsayed, Y. Lu, Y. Wang, X. Lee, T. Lin, N. Thang, H. Wu, S. Haw, K. Wu, M. Lin, K. Chen and L. Chen, *Small*, 2024, **20**, e2400724.